HIGHLIGHT

Two-dimensional transition metal diseleniums for energy storage application: a review of recent developments

Yong-Ping Gao,[a] Xu Wu,[c] Ke-Jing Huang,*[b] Ling-Li Xing,[b] Ying-Ying Zhang[a] and Lu Liu[a]

Two-dimensional transition metal diseleniums (2D-TMDSs) have recently triggered worldwide research interest due to their outstanding properties, such as abundance, low cost, chemical and thermal stability, low framework density and ease of processability. More fascinating is the fact that these materials are extensively used in energy storage (including supercapacitors, lithium ion batteries (LIBs), and sodium ion batteries (SIBs)) and hydrogen storage, and exciting progress has been recently achieved in the synthesis, characterization, device fabrication and functionalization of these 2D-TMDS materials. In this work, the properties of 2D-TMDSs and their use in energy storage are reviewed. In addition, being semiconductors with considerable mobility, TMDSs have been touted as a candidate in next generation electronics, and this review demonstrates the merits of TMDSs by intensive investigations into their use in energy storage. As a result of numerous opportunities for applications and multiple challenges to overcome, this review will be instructive and useful to researchers working in the area of 2D materials as well as scientists and engineers interested in their applications in supercapacitors, LIBs, SIBs and hydrogen storage.

[a] College of Science and Technology, Xinyang University, Xinyang 464000, China
[b] College of Chemistry and Chemical Engineering, Xinyang Normal University, Xinyang 464000, China. E-mail: kejinghuang@163.com; Tel: +86 376 6390611
[c] College of Physics and Electronic Engineering, Xinyang Normal University, Xinyang 464000, China

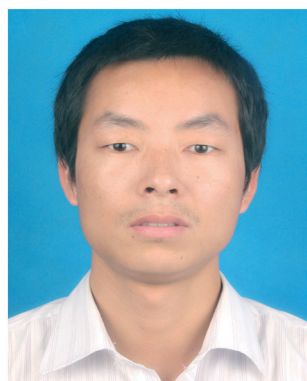## 1. Introduction

Meeting the growing energy demand of the current society, while avoiding resource depletion and environmental pollution, requires the development of high-performance, low-cost and environment-friendly energy storage and production systems.[1–3] Currently, much research effort is focused on the improvement of the performance of energy storage devices,

such as supercapacitors, batteries (especially LIBs and SIBs), and hydrogen storage. In order to accomplish such targets, key aspects are focused on the design of novel materials and the development of synthesis processes that allow precise control over the structural and chemical characteristics of the material, as well as seeking greener and more effective material synthesis processes for the widespread utilization of such devices.

Recently, transition metal dichalcogenides (TMDCs) have been intensively investigated in energy storage fields because of their high theoretical capacity and inexpensiveness together with the abundance of the elements. TMDCs are layered materials consisting of a hexagonal arrangement of transition metal atoms sandwiched between two layers of group six chalcogenide atoms such as S or Se.[4,5] The positions of the elements in the periodic table are highlighted in Fig. 1a.[4] In TMDCs, the transition metal atoms are covalently bonded to a trigonal arrangement of chalcogenides within the same layer while individual layers are held together through non-covalent van der Waals forces. Fig. 1d describes the physical structure for a particular TMDC, MoS_2.[6] Unlike graphene which only has a single molecular structure as it contains only a single element and is a single atom thick, a single layer of TMDC which consists of three layers of atoms (a central transition metal sandwiched between chalcogenides) can exist in two different molecular structures, depending on the relative arrangement of the three atomic layers. Fig. 1b and c describe two molecular structures that a monolayer of TMDC can be in. The trigonal prismatic (D_{3h}) phase has a non-centrosymmetric configuration while the octahedral (O_h) phase, also known as the antiprismatic point group (D_{3d}) phase, has a centrosymmetric configuration.[7]

Many reports, for instance, have described the energy storage of molybdenum disulfides by manufacturing MoS_2 with particular morphologies and sizes[8–12] and MoS_2 with the combination of other electrically conductive matrixes[13–19] including carbon nanotubes, graphene, carbon spheres, and polymers. As a matter of fact, selenium is a d-electron containing member of group 16 with high electrical conductivity (approximately 20 orders of magnitude greater than that of 3 sulphur). However, the electrochemistry of Se in different electrochemical systems is still not fully understood, which may be the greatest hindrance for developing advanced Se electrode materials, and thus requires continuous

Ke-Jing Huang received his PhD in 2006 from Wuhan University. Presently, he is a professor at Xinyang Normal University. His research interests include 2D nanomaterial preparation, supercapacitor electrode materials and electrochemical biosensors.
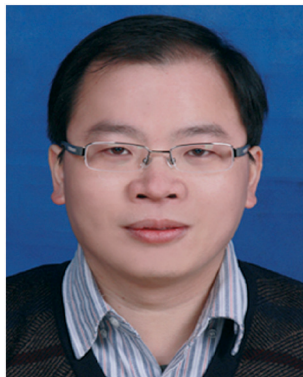
Ke-Jing Huang

Lingli Xing is a master's student at the School of Chemistry and Chemical Engineering, Xinyang Normal University. She received her B.S. at Xinyang University. Her research focuses mainly on micro/nanostructured materials for supercapacitor applications.
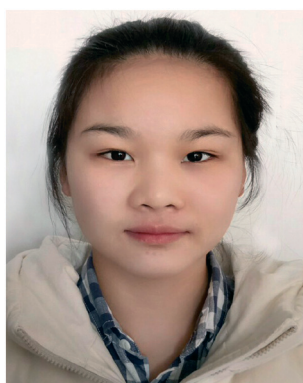
Lingli Xing

Ying-Ying Zhang is a student of chemistry in Xinyang College. Her research focuses mainly on micro/nanostructured materials for supercapacitor applications.

Ying-Ying Zhang

Lu Liu is a student of chemistry in Xinyang College. Her research focuses mainly on micro/nanostructured materials for supercapacitor applications.

Lu Liu
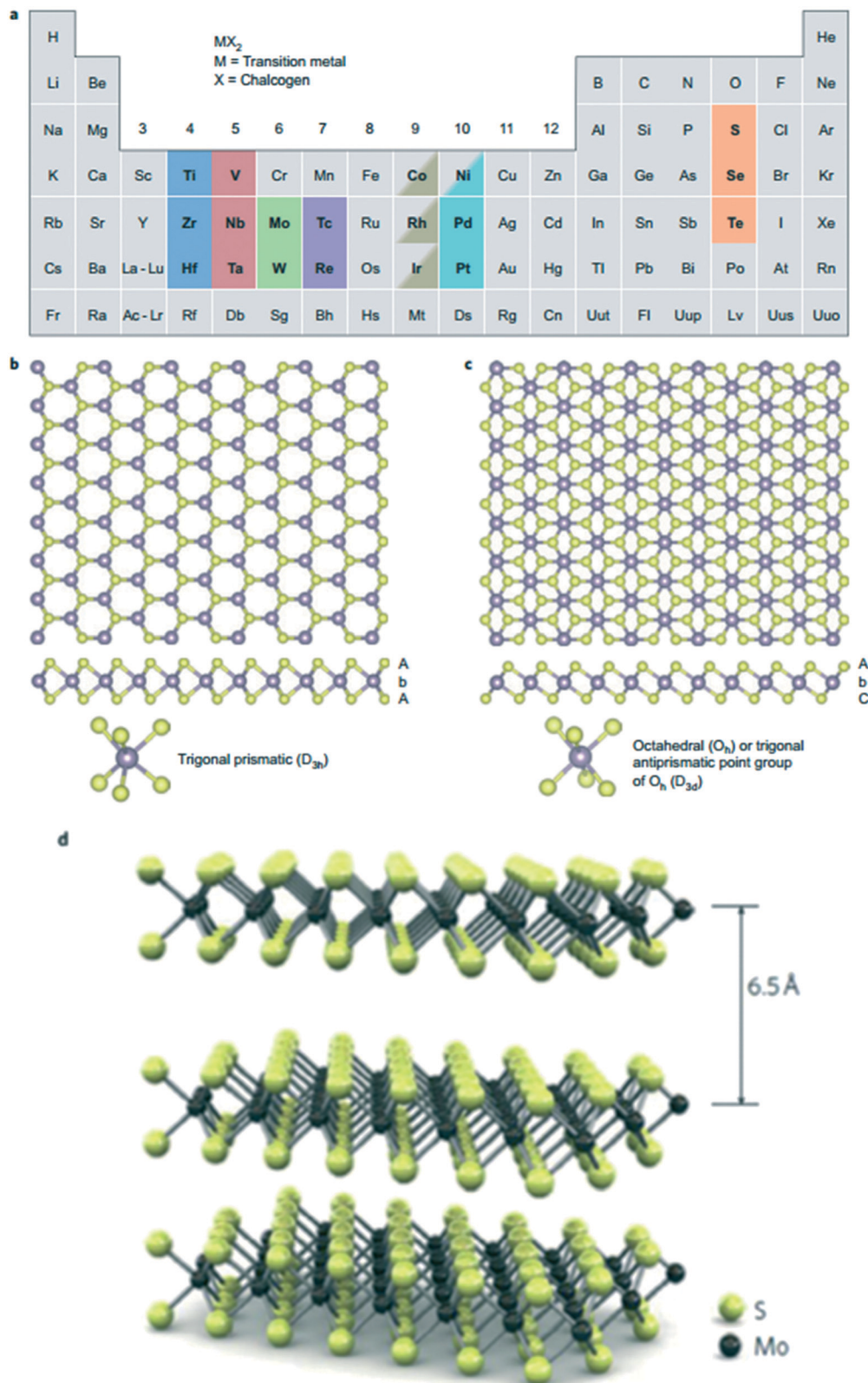
Fig. 1 Structure of monolayer TMDCs. (a) About 40 different layered TMDC compounds exist. The transition metals and the three chalcogen elements that predominantly crystallize in these layered structures are highlighted in the periodic table. Partial highlights for Co, Rh, Ir and Ni indicate that only some of the dichalcogenides form layered structures. c-Axis and section view of single-layer TMDC with trigonal prismatic (b) and octahedral (c) coordination. Atom colour code: purple, metal; yellow, chalcogen. The labels AbA and AbC represent the stacking sequence where the upper- and lower-case letters represent chalcogen and metal elements, respectively. (d) Three dimensional representation of the structure of MoS_2 with single layers being 6.5 Å thick. (a–c) Reproduced with permission.[4] Copyright 2013, Macmillan Publishers Limited. (d) Reproduced with permission.[6] Copyright 2011, Macmillan Publishers Limited. Reproduced with permission.[38] Copyright 2010, American Chemical Society.

investigation. In addition to the electrochemistry, for possible future applications, we have to evaluate several other benchmarks of Se in energy storage applications, which are listed in Table 1 in comparison with S. The density and electronic conductivity of Se are its advantages, while other characteristics raise some concerns (and some unnecessary concerns) about the application prospect of Se-based energy storage materials. On the contrary, Se-based materials have been explored as electrode materials for solar cells[20–22] and rechargeable batteries.[23,24] Two-dimensional transition metal diseleniums (2D-TMDSs), like 2D-TMDCs, are layered materials which can be thinned down to a single layer, albeit being three atoms thick instead of one.[4] 2D-TMDSs have exhibited considerable charge mobility with a semiconducting band gap,[6,7,25] allowing significant intrinsic on–off current ratios.[25] Furthermore, 2D-TMDSs have also shown remarkable physical and optoelectronic properties such as high tensile strength[15] as well as exhibited intrinsic spin–valley polarization of its electronic bands.[25] Thus, 2D-TMDSs have been touted to be a promising component in advanced device technology and optoelectronics. 2D-TMDSs are also focused on the improvement of performance of energy storage devices.

A multitude of articles have focused on the synthesis and applications of 2D-TMDSs, which mainly include top-down and bottom-up means. In top-down processes, they can be fabricated by thinning down bulk TMDS crystals to their constituent layers. The most commonly used method is mechanical exfoliation where an adhesive tape is used to peel off thin layers of TMDSs and deposit them on the desired surface.[32] The crystal quality of the material produced as such is the highest but is greatly limited by the randomness in thicknesses of the flakes that can be obtained as well as its low yield which prevents potential from scaling up. Chemical vapor deposition (CVD) is an important bottom-up technique for growth of 2D-TMDSs, in which solid powders containing the elements present in the TMDS are thermally evaporated and undergo chemical reaction on a solid surface to form the desired TMDS layer in a furnace at high temperatures.[33–35]

2D-TMDSs have attracted crucial interest in multiple energy-related applications due to their processability and the possibility of tuning their textural and structural characteristics to fulfill the requirements of specific applications. Thus, they have an enormous attractiveness to the researchers as outstanding energy storage materials which may take the place of TMDC materials. Huang *et al.*[36] first

reported a simple hydrothermal method to synthesize layered $MoSe_2$ nanosheets on Ni-foam ($MoSe_2$–Ni) for enhanced supercapacitor performance. The $MoSe_2$–Ni displayed faradaic pseudo-capacitance characterization and sufficiently favorable structure stability for sustaining good cycling stability (retaining 104.7% after 1500 cycles) as well as remarkably enhanced specific capacitance (1114.1 F g^{-1} at 1 A g^{-1}). Wang *et al.*[37] successfully synthesized VSe_2/graphene nanocomposites as anode materials for lithium-ion batteries. Keith Share *et al.*[38] primarily demonstrated tungsten diselenide (WSe_2) as an efficient electrode for sodium ion batteries. A high reversible capacity above 200 s^{-1} was observed at 20 mA g^{-1} rate, with over 250 mA h g^{-1} capacity measured in the first sodium extractions. Ultra-thin and porous $MoSe_2$ nanosheets studied by Lei *et al.*[39] were shown in a modified liquid exfoliation method to be efficient electrocatalysts for the hydrogen evolution reaction.

These characteristics have widened the usefulness of 2D-TMDSs to more demanding applications. This review covers the energy-related applications of 2D-TMDSs, with a summary of recent research progress on the development of 2D-TMDSs with more controlled structural and chemical characteristics. Herein, we highlight the applications of 2D-TMDSs in energy storage, such as supercapacitors, LIBs, and SIBs, and hydrogen storage.

2. Use of 2D-TMDSs in energy related applications

Nowadays, an increasing number of researchers are paying attention to 2D-TMDSs. These materials are being researched for their applications in supercapacitors, batteries (especially in LIBs, and SIBs) and hydrogen storage. This section highlights the performance of various 2D-TMDSs used in different energy related applications.

2.1. Supercapacitors

The recent development of modern electronic devices and the progressive research on renewable energy-based electrochemical energy conversion systems have fuelled the drive toward advanced high-performance energy storage devices. Among the various types of energy storage devices, supercapacitors have been recognized as one of the most promising candidates for high-power applications such as hybrid-electric vehicles, portable electronics, digital

Table 1 Comparison of several parameters of S and Se. Reproduced with permission.[26] Copyright 2015, American Chemical Society

	Sulfur	Selenium
Density (g cm^{-3})[27]	2.07 (α-S)	4.8 (t-Se)
Electrical resistivity (μΩ cm)[28]	2×10^{23} (20 °C)	1.2 (0 °C) the text runs thus
World production (2012, t)[29]	68 100 000	2240
Toxicity (LD50 oral, rat, g kg^{-1})[30]	3	6.7
Melting point (°C)[30]	114	217–222
Autoignition temperature (°C)[30]	235	n/a
Price (2013, $ per kg)[31]	0.124 (mine and/or plant)	77 (refined)

communications, and renewable-energy systems due to their attractive properties, including high power density, long cycle life, fast charge/discharge rate, and better safety.[40–45] In general, supercapacitors can be classified into two categories based on the charge storage mechanism: electrochemical double layer capacitors (EDLCs: where ion adsorption occurs at the electrode/electrolyte interface) and pseudocapacitors (involving fast faradaic charge transport reactions).[44,46,47] Electrode materials for EDLCs are usually carbon-based materials such as activated carbon, carbon nanotubes (CNTs), carbon nanofibers (CNFs) and graphene.[48–51] However, the specific capacitance of carbon-based materials is generally low due to the limited specific surface area and nonuniform pore size distribution of these materials, which in turn limits the effective utilization of these electroactive materials in supercapacitors.[52,53] On the other hand, transition metal oxides,[54–56] metal hydroxides,[57–59] conducting polymers,[60] and TMDCs[61,62] have been widely used as electrode materials for pseudocapacitors due to their much higher specific capacitance. Although pseudocapacitors generally have a high specific capacitance, the poor stability and low conductivity of the pseudocapacitive materials limit their practical application in the energy storage field.[63,64] In order to overcome these issues as well as to achieve an enhanced electrochemical performance, novel hierarchical hybrid nanostructures combining EDLCs and pseudocapacitors have emerged, where these systems have a large surface area, good electrical conductivity, and a short path for ion diffusion.

2.1.1. MoSe₂. Recently, TMDCs, MX_2 (M = Mo, W; X = S, Se), with a layered structure (analogous to graphene) have emerged as one of the most prominent candidates for energy storage, catalysis, photo-transistors, and sensor systems due to their unique crystal structures and diverse material properties.[65–68] In these materials, metals and chalcogens interact *via* strong chemical bonds in the molecular layers, whereas the individual layers interact *via* weak van der Waals forces, forming a graphene-like layered structure, as shown in Fig. 1. This structure is beneficial for the insertion and extraction of a variety of electrolyte ions and can be exploited in the field of energy storage.[69,70] Interestingly, similar to MoS_2, $MoSe_2$, is an important narrow-bandgap semiconductor that has a layered structure (Se–Mo–Se), which might be a good choice for energy storage devices.[71,72] Furthermore, the interlayer spacing of $MoSe_2$ (0.646 nm) is larger than that of graphite (0.335 nm) and MoS_2 (0.615 nm).[70] Therefore, as a representative of TMDS, $MoSe_2$ is considered as one of the most promising electrode materials for supercapacitors, and some studies have been carried out on the electrochemical performance of supercapacitors employing $MoSe_2$.[73–76] The reaction mechanism of $MoSe_2$ nanosheets resulting from the faradaic electrochemical process is shown in eqn (1). Although $MoSe_2$ has been applied in energy storage, its poor electrical conductivity, which is similar to that of other metal oxides, hinders its electrochemical performance and practical implementation.

$$(MoSe_2) + H^+ + e^- \leftrightarrow MoSe - SeH^+ \tag{1}$$

A commonly employed strategy to further enhance the electrochemical performance of $MoSe_2$ involves the design of a hybrid nanostructure with a carbon matrix. Compared with other carbon materials, graphene is considered as the most auspicious matrix to support host materials because of its intriguing advantages, including a large specific surface area, superior electrical conductivity, good chemical stability, and excellent mechanical flexibility.[77–80] Due to its outstanding properties, graphene shows excellent potential as an electrode material for high-performance supercapacitors. Moreover, the graphene nanosheets in the hybrid nanostructure serve as a powerful support, which can provide better electrical conductivity, curtail aggregation of the target nanomaterials, and shorten the transport paths for effective mass and charge transport. Furthermore, grafting with $MoSe_2$ can also effectively reduce restacking of the graphene nanosheets, thereby facilitating complete utilization of the surface active sites and further accelerating ion diffusion. Hence, it is expected that the hybrid nanostructure of $MoSe_2$/graphene, in which $MoSe_2$ nanosheets are uniformly distributed in the graphene matrix, should be an effective and competitive platform to achieve outstanding electrochemical performance by combining the advantages of the individual components while exploiting their synergistic effects in the electrode matrix.[70]

Up to now, some studies have explored the use of pristine $MoSe_2$ and graphene/$MoSe_2$ composites for energy storage applications. For instance, Huang *et al.*[81] first reported the preparation of $MoSe_2$–graphene grown on Ni-foam ($MoSe_2$–graphene/Ni) (Fig. 2). By taking advantage of its porous layered structure and vertically aligned orientation, $MoSe_2$–graphene/Ni displayed a high performance when used as the supercapacitor electrode material. Balasingam *et al.*[82] synthesized a large quantity of few-layered $MoSe_2$ nanosheets using a facile hydrothermal method. The $MoSe_2$ nanosheets were investigated for supercapacitor applications in a symmetric cell configuration. The result exhibited a maximum specific capacitance of 198.9 F g⁻¹ and the symmetric device showed 49.7 F g⁻¹ at a scan rate of 2 mV s⁻¹. A capacitance retention of approximately 75% was observed even after 10 000 cycles at a high charge–discharge current density of 5 A g⁻¹. The following year, Balasingam *et al.*[83] introduced a facile, low-cost, and scalable approach for synthesis of $MoSe_2$/graphene nanosheet electrode materials *via* a hydrothermal method. The hybrid nanostructure materials exhibited a maximum specific capacitance of 211 F g⁻¹ at a scan rate of 5 mV s⁻¹ and a good capacitance retention ratio of 180% even after 10 000 cycles at a current density of 5 A g⁻¹. A facile hydrothermal strategy was applied by Liu *et al.*[84] to prepare net-like $MoSe_2$–acetylene black (AB), tailoring the interior structure by using Ni substrate. The $MoSe_2$–AB nanostructures constructed with $MoSe_2$ ultrathin nanosheets were applied as supercapacitor electrode materials. As expected, the net-like $MoSe_2$–AB composites exhibited a high specific capacitance (2020 F g⁻¹ at 1
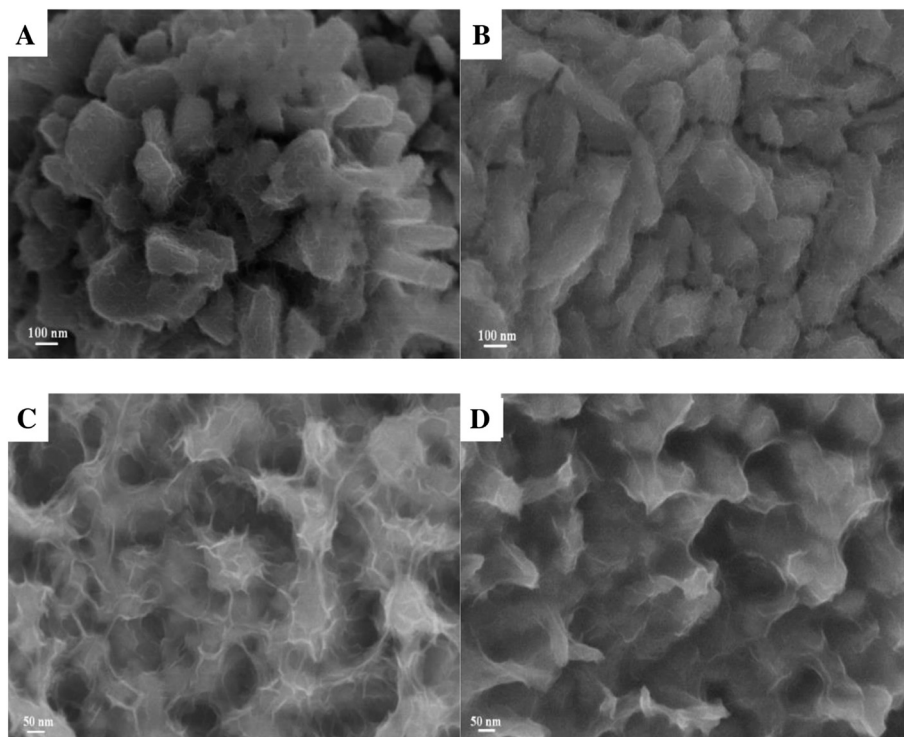
Fig. 2 SEM images of MoSe$_2$–graphene/Ni with various MoSe$_2$/graphene mass ratios: (A) 5 : 1; (B) 6 : 1; (C) 7 : 1 and (D) 8 : 1. Reproduced with permission.[81] Copyright 2015, Elsevier Ltd.

A g^{-1}) and good cycling stability (107.5% after 1500 cycles) due to their unique architecture. Therefore, the 2D MoSe$_2$ nanosheets exhibit a high specific capacitance and good cycling stability, which makes them a promising electrode material for supercapacitor applications.

2.1.2. Others. In addition to MoSe$_2$, many other TMDSs have attracted particular attention in the energy research community. Take Co$_{0.85}$Se for example. As early as 2013, Wang et al.[85] successfully synthesized polycrystalline Co$_{0.85}$Se nanotubes by using Co(CO$_3$)$_{0.35}$Cl$_{0.20}$(OH)$_{1.10}$ nanorods as a precursor through a solvothermal process. The as-prepared Co$_{0.85}$Se nanotubes showed efficient catalytic performance for the decomposition of hydrazine hydrate at room temperature. The values of specific capacitance with respect to charge–discharge cycle number (up to 2000 cycles) at a current density of 1 A g^{-1} were determined; the specific capacitance of Co$_{0.85}$Se electrode was increased from 216 to 238 F g^{-1} after the initial 100 cycles. With increasing cycle number, the specific capacitance slowly decreased and a deterioration of about 9.7% of the maximum specific capacitance occurred after the next 1900 cycles. The impedance of the Co$_{0.85}$Se nanotube electrode after the 1st and 50th cycles was measured. In the high frequency domain, a small semicircle is observed, and in the low frequency section, the plot tends to be a straight line where the imaginary part of the impedance rapidly increases. In the ensuing year Banerjee et al.[86] fabricated a supercapacitor electrode with a Co$_{0.85}$Se hollow nanowire (HNW) array, which was synthesized by wet chemical hydrothermal selenization of initially grown cobalt hydroxyl

carbonate nanowires on conductive carbon fiber paper. The dense self-organized morphology of Co$_{0.85}$Se HNWs was revealed by scanning/transmission electron microscopy. The as-synthesized Co$_{0.85}$Se HNWs possessed a high pseudocapacitive property with high capacitance retention and high durability. The areal capacitance value was seen to vary from 929.5 to 600 mF cm^{-2} (60% retention) as the current density was increased from 1 to 15 mA cm^{-2}, with an increase of a factor of 15. Based on mass loading, this corresponded to a very high gravimetric capacitance of 674 (for 2 mA cm^{-2} or 1.48 A g^{-1}) and 444 F g^{-1} (for 15 mA cm^{-2} or 11 A g^{-1}) in a full-cell configuration with the Co$_{0.85}$Se HNWs as the cathode and activated carbon as the anode (asymmetric configuration); promising results were obtained. Peng et al.[87] successfully assembled a novel asymmetric supercapacitor (ASC) based on petal-like cobalt selenide (Co$_{0.85}$Se) nanosheets as the positive electrode and nitrogen-doped porous carbon networks (N-PCNs) as the negative electrode in a 2 M KOH aqueous electrolyte. The Co$_{0.85}$Se/N-PCN ASC device possessed an extended operating voltage window of 1.6 V, high energy density of 21.1 W h kg^{-1} at a power density of 400 W kg^{-1} and outstanding cycling stability (93.8% capacitance retention after 5000 cycles) in an aqueous electrolyte. Yu et al.[88] reported hierarchical CoSe$_2$ nanostructures (see Fig. 3) successfully grown on conductive carbon fabrics with robust adhesion by a facile two-step method. The hierarchical CoSe$_2$ architectures exhibited a large specific capacitance of 332 mF cm^{-2} at a current density of 1 mA cm^{-2}. After charging/discharging for 5000 cycles, the electrode still showed superior stability
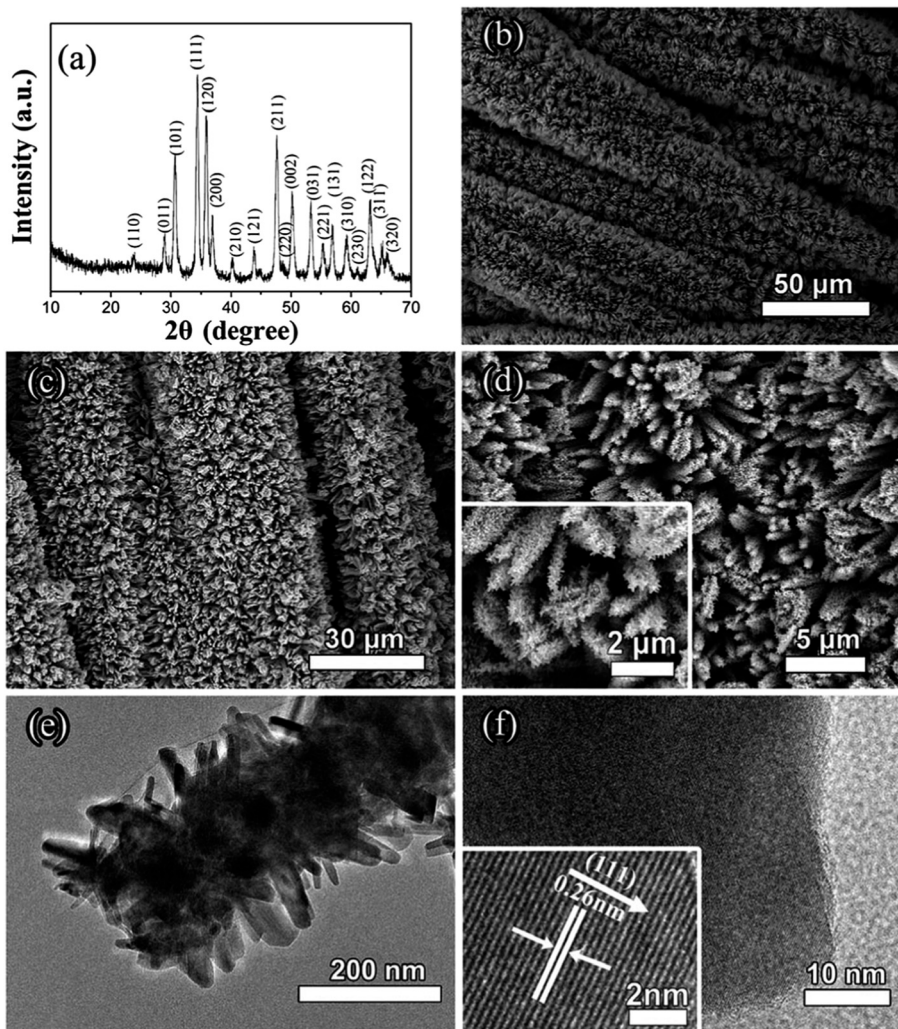
Fig. 3 (a) XRD pattern of CoSe₂ products. (b) SEM image of the Co₃O₄ nanowire array on carbon cloth. (c and d) SEM images of CoSe₂ on carbon cloth. (e) TEM image of CoSe₂ products. (f) HRTEM image of CoSe₂. Reproduced with permission.[88] Copyright 2015, The Royal Society of Chemistry.

with the capacity retention of about 95.4%. Pazhamalai *et al.*[89] demonstrated the use of CuSe₂ nanoneedles grown on copper foil as a binder-free electrode for supercapacitors. Zhang *et al.*[90] claimed that SnSe₂ nanodisks were promising candidate materials for use in high-performance, flexible, all-solid-state supercapacitors. Wang *et al.*[91] synthesized hierarchical GeSe₂ nanostructures by using a chemical vapor deposition method, which exhibited a specific capacitance of 300 F g⁻¹ at a current density of 1 A g⁻¹, and was rarely observed for other electro-active metal chalcogenides. On the basis of the excellent electronic properties of 2D layered crystal structures and their unique mechanical flexibility,[92,93] synthesizing 2D-TMDS nanostructures and exploring their applications in supercapacitors seem to be of great importance.

2.2. Batteries

2D-TMDS nanomaterials, including multi-layered nanosheets of layered compounds have been widely investigated and

employed in energy storage applications.[94,95] Their particular mechanical, optical, and electrical properties are closely bound up with their physico-chemical uniqueness. The TMDS compounds possess a structure similar to graphite, consisting of three atom layers in which the layers of metal atoms are sandwiched between two chalcogen layers. Therefore, Li-ions and Na-ions are easily intercalated and deintercalated from this layered structure because of the weak van der Waals forces. Thus, layered TMDS compounds have been considered as promising anodes for lithium and sodium storage.[96]

2.2.1. Lithium ion batteries. Since the commercialization of LIBs by Sony Energytech in 1991, LIBs have become the prominent energy storage technology in modern applications. LIBs have not only been widely used in portable electronic devices, but also are now powering hybrid electric and plug-in electric vehicles and show promise to be applied in stationary energy storage systems. Batteries for these large-scale applications require a significant improvement in the lithium

storage capacity.[97,98] LIBs have been extensively studied to obtain more efficient storage systems so as to satisfy the growing demands of higher power and energy density for large-scale rechargeable batteries. Since the traditional prevailing graphitized carbon anode materials could not satisfy the increasing demands for high power and high energy because of low theoretical capacity (372 mA h g^{-1}) and poor rate performance,[99] many efforts have been made in the development of new anode materials with high performance and high capacity.[100]

Layer structured TMDS are of great interest in energy storage because their crystal structure can be easily utilized for the reversible storage of lithium *via* electrochemical intercalation, making them good candidates for LIB applications. Recently, a great amount of research has focused on the synthesis and application of various nanostructured TMDS materials in electrochemical lithium storage due to the high theoretical capacity and excellent cycling performance. Many works related to the use of flexible TMDS nanostructure composites in LIBs can be found in the literature. As early as 2006, Xue *et al.*[101] successfully synthesized NiSe$_2$ thin film by reactive pulsed laser deposition and investigated its electrochemistry with lithium for the first time. The reversible discharge capacities of NiSe$_2$/Li cells cycled between 1.0 V and 3.0 V were found in the range of 314.9–467.5 mA h g^{-1} during the first 200 cycles. Galvanostatic cycling measurements and cyclic voltammetry (CV) were used to examine the electrochemical behavior of the NiSe$_2$/Li cell. A large reversible discharge capacity of 351.4 mA h g^{-1} of the NiSe$_2$/Li cell was achieved. By using *ex situ* XRD, TEM and SAED measurements, a complicated electrochemical reaction mechanism of NiSe$_2$ with lithium consisting of three reversible conversions with the intermediates β-NiSe and Ni$_3$Se$_2$ and metal nickel was first proposed. The two redox active centers of both cation (nickel) and anion (selenium) in NiSe$_2$ were revealed. The high reversible capacity and good cycling stability of NiSe$_2$ thin film electrode make it one of the promising storage energy materials for future rechargeable lithium batteries. Shi *et al.*[102] synthesized highly ordered mesoporous crystalline MoSe$_2$ using mesoporous silica SBA-15 as a hard template *via* a nanocasting strategy (see Fig. 4). Selenium powder and phosphomolybdic acid (H$_3$PMo$_{12}$O$_{40}$) were used as Se and Mo sources, respectively. The obtained products had a highly ordered hexagonal mesostructure and a rod-like particle morphology, analogous to the mother template SBA-15. The UV-vis-NIR spectrum of the material showed a strong light absorption throughout the entire visible wavelength region. The direct bandgap was estimated to be 1.37 eV. The high surface area MoSe$_2$ mesostructure showed remarkable photocatalytic activity for the degradation of rhodamine B, a model organic dye, in aqueous solution under visible light irradiation. In addition, the synthesized mesoporous MoSe$_2$ possessed a reversible lithium storage capacity of 630 mA h g^{-1} for at least 35 cycles without any notable decrease. Wang *et al.*[103] synthesized MoSe$_2$ nanocrystals *via* a facile thermal-decomposition process. As the anode, the nanocrystalline MoSe$_2$ yielded the
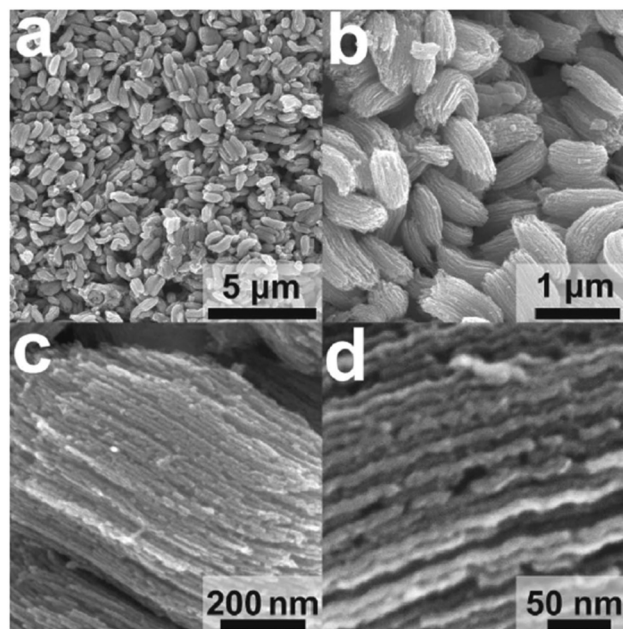

Fig. 4 (a–d) SEM images of the synthesized mesoporous MoSe$_2$ materials using SBA-15 as the template *via* a nanocasting method. Reproduced with permission.[102] Copyright 2013, WILEY-VCH Verlag GmbH & Co. KGaA, Weinheim.

initial discharge and charge capacities of 782 and 600 mA h g^{-1} at a current of 0.1 C in a voltage of 0.1–3 V. Kang *et al.*[104] prepared SnSe nanosheets *via* a reaction at the oil–water interface in a solvothermal process at low temperature (130 °C), which did not involve any templates and amines such as oleylamine. X-ray diffraction, transmission electron microscopy, absorption spectroscopy and nitrogen adsorption were used to characterize the products. The results indicated that the SnSe nanosheets obtained adopted a square-like morphology with lateral dimensions of approximately 120 nm × 120 nm and possessed high crystallinity. Moreover, their electrochemical performance, as an anode material, was evaluated by galvanostatic discharge–charge tests, showing that the as-prepared SnSe nanosheets exhibited a high initial discharge capacity of 1009 mA h g^{-1} as a potential energy storage material. Klavetter *et al.*[105] showed the high tap density microparticles of selenium-doped germanium to be a high efficiency, stable cycling anode material in LIBs. In particular, Im *et al.*[106] reported the novel synthesis of GeSe$_x$ and SnSe$_x$ (x = 1 and 2) nanocrystals by a gas-phase laser photolysis reaction and their excellent reversible capacity for LIBs. SnSe$_x$ exhibited higher rate capabilities compared to GeSe$_x$. *Ex situ* X-ray diffraction and Raman spectroscopy revealed the cubic–tetragonal phase conversion of Ge and Sn upon lithiation/delithiation to support their distinctive lithium ion battery capacities. Chen *et al.*[107] synthesized an ordered mesoporous WSe$_2$ with a crystalline framework by a nanocasting method using mesoporous silica SBA-15 as a hard template. The mesoporous WSe$_2$ displayed good electrochemical properties with a high reversible capacity (530 mA h g^{-1}) and stable cycling performance. Another form is TMDS and its

nanostructured composite for LIBs. Yao *et al.*[108] synthesized a self-assembled $MoSe_2$ nanolayer/reduced graphene oxide ($MoSe_2$/rGO) foam using a hydrothermal method. The specific capacity of the $MoSe_2$/rGO anode could reach up to 650 mA h g^{-1} at a current rate of 0.1 C in the voltage range 0.01–3.0 V (*vs.* Li/Li$^+$), which was higher than the theoretical capacity of $MoSe_2$ (422 mA h g^{-1}). Additionally, the fabricated half cells have shown good rate capability and long cycling stability with 10.9% capacity loss after 600 cycles under a current density of 0.5 C. Ma *et al.*[109] successfully synthesized ultrathin $MoSe_2$/graphene hybrids through a facile ionic liquid-assisted hydrothermal approach. The resultant hybrids were characterized by X-ray diffraction (XRD), field emission scanning electron microscopy (SEM) and high-resolution transmission electron microscopy (HRTEM). It was revealed that the $MoSe_2$ nanosheets in the hybrids exhibited a graphene-like few-layered structural characteristic of 2–3 layers and were well dispersed and anchored on the large flexible graphene sheets. Furthermore, $MoSe_2$@HCNF (hollow carbon nanofiber) composites,[110] $MoSe_2$@SWCNT (single-walled carbon nanotube) composites,[111] $MoSe_2$@C composites,[112] $SnSe_2$@graphene composites,[113] SnSe@CNF (carbon matrix) composites,[114] SnSe@C composites,[115] VSe_2/graphene composites[116] and ZnSe/C composites[117] were prepared and used for LIBs, exhibiting excellent electrochemical properties.

2.2.2. Sodium ion batteries. LIBs have become the prominent energy storage technology in modern applications such as electric vehicles and portable electronics.[118] As battery demand increases, alternative earth-abundant battery materials are required to achieve progress both in performance and in cost. Recently, SIBs have been considered to be attractive alternatives to LIBs for energy storage systems owing to the abundant reserves and low cost of sodium and have gained more and more attention. In many cases, this enables direct application of knowledge gained from LIB research to be readily applied in SIB systems since electrode materials, such as transition metal oxides, have Na equivalents.[119,120] However, there is a main drawback because the size of Na$^+$ (1.02 Å) is larger compared to Li$^+$ (0.76 Å), which hinders their expansion. The energy density of SIBs is slightly lower than that of LIBs because the reversible capacity and operating voltage of currently reported electrode materials in SIBs are lower in comparison. As an example, graphite, which is the benchmark anode material for LIBs, stores over 10 less Na ions per carbon atom than Li.[120,121] This underlines the need for the exploration of new electrode materials for SIBs that can be competitive in performance with commercially available lithium-ion cells.[122]

In conclusion, it is not easy to replace LIBs with SIBs because the cost per energy stored ($ per W h) of SIBs does not provide much advantage.[123] Therefore, new electrode materials having higher reversible capacities are necessary for increasing the energy density of SIBs. Recently, there have been notable achievements in the development of high-capacity 2D-TMDS based materials in SIBs. For example, Ko *et al.*[124]

reported pioneering work on the synthesis of yolk–shell-structured $MoSe_2$ microspheres *via* a simple selenization process, as shown in Fig. 5. The prepared $MoSe_2$ yolk–shell microspheres were aggregates of thin-layered nanosheets and exhibited excellent Na-ion storage properties. The yolk–shell-structured $MoSe_2$ and MoO_3 microspheres delivered initial discharge capacities of 527 and 465 mA h g^{-1} in the voltage range of 0.001–3 V *vs.* Na/Na$^+$ at a current density of 0.2 A g^{-1}, respectively, and their discharge capacities after 50 cycles were 433 and 141 mA h g^{-1}, respectively. Wang *et al.*[125] synthesized $MoSe_2$ nanoplates for high performance SIBs. Kim *et al.*[126] first examined SnSe as an anode material for SIBs. WSe_2 was demonstrated as an efficient electrode for SIBs for the first time by Share *et al.*[127] Recently, much research on energy storage has examined TMDS and its nanostructured composite for SIBs. Zhang *et al.*[128] decorated ultrathin molybdenum diselenide nanosheets on the surface of multi-walled carbon nanotubes (MWCNTs) *via* a one-step hydrothermal method. The $MoSe_2$@MWCNT composites delivered a reversible specific capacity of 459 mA h g^{-1} at a current of 200 mA g^{-1} over 90 cycles, and a specific capacity of 385 mA h g^{-1} even at a current rate of 2000 mA h g^{-1}, which was better than that of $MoSe_2$ nanosheets. Choi *et al.*[129] exhibited the superior sodium-ion storage properties of $MoSe_2$/CNT (carbon nanotube) composite balls to that of bare $MoSe_2$. Yang *et al.*[130] synthesized porous hollow carbon spheres (PHCS) decorated with $MoSe_2$ nanosheets ($MoSe_2$@ PHCS) *via* a three-step process. Zhang *et al.*[131] synthesized a flexible $MoSe_2$/CF (carbon fibre) composite by a simple solvothermal method. Zhang *et al.*[132] synthesized SnSe/carbon nanocomposite by high energy ball milling as an anode material for SIBs. Similarly, nanostructured WSe_2/carbon composites were synthesized by Zhang *et al.*[133] as anode materials for SIBs.

2.3. Hydrogen storage

Hydrogen, a clean renewable energy source, has been vigorously proposed as the promising future energy carrier in the hydrogen-economy paradigm.[134–138] Recently, the generation of hydrogen by efficiently splitting water initiated either by light or by electricity has attracted a great deal of attention due to its cleanliness and low cost.[139–146] Hydrogen evolution reaction (HER) is the essential step in water electrolysis where hydrogen is produced by reduction of protons. Both efficient and economical electrocatalysts for HER are required to achieve high current densities at low overpotentials. Although some precious metals and their alloys, such as Pt and Pd, have a exhibited high catalytic activity for HER, the high cost and low natural abundance restrict their practical applications in the industrial production of hydrogen.[147]

Recent studies have proven that newly emerging two-dimensional molybdenum diselenide is a promising noble-metal-free electrocatalyst for HER. Take $MoSe_2$ for example. It is a newly emerging catalyst and most used owing to its low cost, high chemical stability, and excellent electrocatalytic
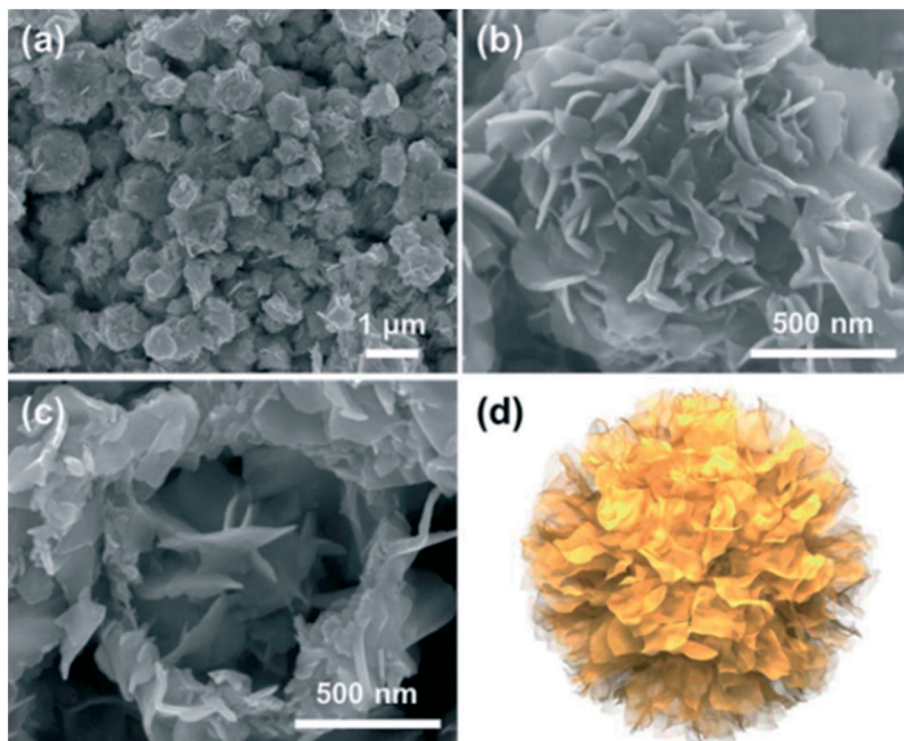
Fig. 5 Morphologies of the hierarchical MoSe$_2$ yolk–shell microspheres: (a and b) FE-SEM images, (c) FE-SEM image of the fractured microsphere, and (d) schematic illustration of the microsphere. Reproduced with permission.[124] Copyright 2013, The Royal Society of Chemistry.

activity.[148–152] Similar to the catalytic mechanism of MoS$_2$, the electrocatalytic HER activity of MoSe$_2$ depends strongly on its active selenium edge sites, while its basal planes are catalytically inert.[153] Density functional theory calculations reveal that the Gibbs free energy for atomic hydrogen adsorption on MoSe$_2$ edges is closer to thermoneutral than that on MoS$_2$, with an H coverage of about 75% on the edge under operating conditions, which is also higher than that of MoS$_2$ reported in the literature. The consistency between the experimental and computational results indicates that MoSe$_2$ nanosheets have potential to be a better HER catalyst than their MoS$_2$ counterpart. Therefore, reducing the size of MoSe$_2$ down to nanoscale and increasing the exposure of its active edges can boost the catalytic activities of MoSe$_2$. It is reported that the vertically aligned MoSe$_2$ molecular layers on curved and rough surfaces such as Si nanowires and carbon microfibers possess maximally exposed active edge sites and thereby exhibit large exchange current densities in HER.[154] In addition to the exposure of active edge sites, electrical conductivity is another key factor influencing the HER performance. However, the poor conductivity between two adjacent van der Waals bonded layers of MoSe$_2$ would significantly suppress their overall HER rate. In this regard, preparation of uniformly distributed MoSe$_2$ nanostructures with more exposed selenium edges on a conductive substrate is an effective strategy to enhance its electrocatalytic performance for HER. For example, Kong et al.[155] described a two-step reaction for preparing electrodes composed of CoSe$_2$ nanoparticles grown on carbon fiber paper (see Fig. 6). The

electrode exhibited excellent catalytic activity for HER in an acidic electrolyte (100 mA cm^{-2} at an overpotential of 180 mV). Stability testing through long-term potential cycles and extended electrolysis confirmed the exceptional durability of the catalyst. Zhao et al.[156] presented a one-pot colloidal route to synthesize VSe$_2$, a new type of metallic single-layer nanosheet. The about 0.4 nm thick VSe$_2$ single layer nanosheets possessed an extraordinary electrocatalytic HER performance with a low onset overpotential of 108 mV, a small Tafel slope of 88 mV per decade, and an exceptional overpotential of 206 mV at a current density of 10 mA cm^{-2}. In addition, many researchers were fascinated by other TMDSs, such as MoSe$_2$ (ref. 157–175) and WSe$_2$.[159,162,170,173–175] Carbon materials, including graphene, CNTs, CNFs, activated carbon, carbon aerogels (CAs), and carbon fiber aerogel (CFA) cloth, etc., are ideal substrates for loading MoSe$_2$ to improve its electrocatalytic activity[175–181] owing to the unique physicochemical properties and excellent conductivity of these carbon materials. For example, Huang et al.[173] synthesized a unique hierarchical nanostructure of few-layered MoSe$_2$ nanosheets perpendicularly grown on CNTs through a one-step solvothermal reaction. This rationally designed architecture based on a highly conductive CNT substrate possessed fully exposed active edges and open structures for fast ion/electron transfer, thus leading to a remarkable HER activity with a low onset potential of −0.07 V vs. reversible hydrogen electrode, a small Tafel slope of 58 mV per decade and excellent long-cycle stability. Zhang et al.[157] reported MoSe$_2$@CFA, which exhibited excellent electrochemical activity as a HER electrocatalyst
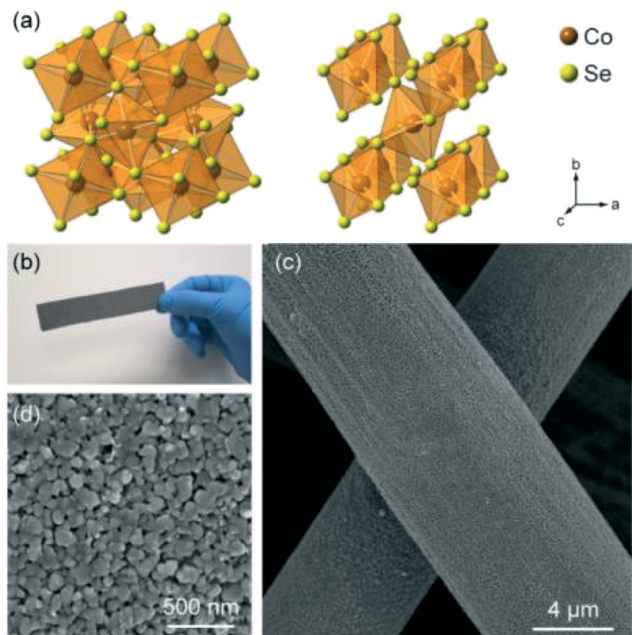
Fig. 6 (a) Crystal structure of $CoSe_2$ in cubic pyrite-type phase (left) and orthorhombic marcasite-type phase (right), in which Co and Se are displayed in orange and yellow, respectively. (b) Photograph of as-prepared $CoSe_2$ catalyst on a piece of 1.5 cm × 10 cm carbon fiber paper. (c) SEM image of a layer of $CoSe_2$ catalyst grown on carbon fiber paper. (d) High-resolution SEM image revealing the structure of $CoSe_2$ coating, consisting of nanoparticles in dimensions of tens of nanometers. Reproduced with permission.[155] Copyright 2014, American Chemical Society.

with a small onset potential of −0.104 V *vs.* reversible hydrogen electrode and a small Tafel slope of 62 mV per decade, showing its great potential as a next-generation Pt-free electrocatalyst for HER. Tang *et al.*,[72] Liu *et al.*,[165] and Jia *et al.*[182] reported the synthesis of $MoSe_2$@graphene. The number of layers of the $MoSe_2$ nanosheets was typically <10. HER studies showed that the onset potentials of $MoSe_2$ and $MoSe_2$/graphene hybrids were only 0.15 V *vs.* RHE and 0.05 V *vs.* RHE, respectively, and about 20–30 mV lower than those of MoS_2 and its graphene hybrids. All results indicated that $MoSe_2$@graphene composite film had potential to be a better catalyst for HER. Therefore, due to their high chemical stability, low cost, high-capacity, and excellent electrocatalytic activity, 2D-TMDS materials have become a type of emerging catalyst and have been used extensively in HER.

3. Summary and outlook

Since the Nobel Prize was awarded for graphene in 2010, there has been considerable research in the field of 2D materials. One particular class of layered 2D materials, TMDCs, is receiving increased interest in applications in energy storage. In recent years, 2D-TMDSs, as a substitute for TMDCs, have attracted more attention in many energy-related applications due to their abundance, chemical and thermal stability, processability and the possibility of tuning their textural and structural characteristics to fulfill the requirements of spe-

cific applications. The application of these materials has been extensively researched as energy storage in supercapacitors, LIBs, SIBs, and hydrogen stores.

2D layer-structured TMDSs have been recognized to have high electrochemical activity, which is due to their unique metallic conductivity, multiple available oxidation states and special geometric structures with weak interlayer van de Waals coupling. Some TMDSs, including $MoSe_2$, $CoSe_2$, and WSe_2, are mainly investigated as novel positive electrode materials for supercapacitors in view of their fascinating physicochemical properties. The development of novel electrodes with more energy and power density for supercapacitor applications has been an emerging area of interest during the recent decade. Similarly, Li-ions and Na-ions are easily intercalated and deintercalated from the layered structure because of the weak van der Waals forces. Thus, layered TMDS compounds have been considered as a promising anode for lithium and sodium storage. Synthesizing new 2D layer-structured TMDSs that have suitable and stable crystal structures as well as good electron/ion conductivities to accommodate long term efficient Li/Na-ion intercalation and deintercalation will be of great significance. On the other hand, constructing composites (*e.g.*, 2D layer-structured TMDS and carbon composite) to utilize the synergistic effect of components is another strategy to promote their lithium/sodium storage capability. As a clean and renewable energy source, hydrogen has a far-reaching significance for the sustainable development of environment and energy. Economical and efficient electrocatalysts for HER are the target of scientific research workers. But at the same time, these require high current densities at low overpotentials. Although some precious metals and their alloys have exhibited high catalytic activity for HER, the low natural abundance and high cost set a limit to their practical applications in industrial production of hydrogen. Due to their high chemical stability, low cost, high-capacity, and excellent electrocatalytic activity, 2D-TMDS materials have become a type of emerging catalyst and have been used potentially in HER. Thus, assembling non-precious 2D-TMDS materials or composites with rich active edges and excellent electron/ion transfer paths to obtain catalysts with high HER activity and can be operated in different systems to replace the current precious catalyst will be the future research directions. In a word, further research on 2D-TMDS materials is needed for clear understanding and as an effective measure to apply in energy storage.

Layered TMDS materials have been known and studied for decades, but their properties as atomically thin, 2D forms are a relatively new and exciting area in nanotechnology, with many promising applications in energy storage. The large bandgaps seen in several members of the TMDS family make them attractive channel materials in logic transistors, and the direct bandgaps in several single-layer TMDSs open up many prospects in energy storage. In studying the physics and chemistry of 2D-TMDSs, researchers will be able to draw upon the previous research on the bulk TMDS intercalation chemistry, material processing and characterization, along

with techniques for device fabrication and nanoscale characterization developed with graphene and other nanostructured materials. But 2D-TMDSs have many distinctive properties that are not seen in other material systems. When researchers learn more about them, there are sure to be unexpected and exciting applications. In the next few years, progress in this field will require advances in scalable and controllable sample preparation to make large amounts of atomically thin and uniform TMDS layers, either in solution or on substrates. For solution-phase preparation, the challenges include controlling the area and thickness of either exfoliated or chemically grown flakes and finding new methods and chemicals that can efficiently and safely produce these materials in large scale. For solid-state samples, crystal growth methods need to be improved to achieve large areas, large grain sizes, uniformity and control of layer number. Access to high-quality samples will enable more researchers to better understand the physical and chemical properties of TMDS, as well as to pursue a wider variety of applications. The properties and applications of 2D-TDMS materials are a relatively new but exciting and rapidly expanding area of research.

Acknowledgements

References

1 M. Sun, H. J. Liu, J. H. Qu and J. H. Li, *Adv. Energy Mater.*, 2016, **6**, 1600087–1600120.

2 T. Lu, S. Dong, C. Zhang, L. Zhang and G. Cui, *Coord. Chem. Rev.*, 2017, **332**, 75–99.

3 G. Zhang, H. J. Liu, J. H. Qu and J. H. Li, *Energy Environ. Sci.*, 2016, **9**, 1190–1209.

4 M. Chhowalla, H. S. Shin, G. Eda, L. J. Li, K. P. Loh and H. Zhang, *Nat. Chem.*, 2013, **5**, 263–275.

5 H. Schmidt, S. F. Wang, L. Q. Chu, M. L. Toh, R. Kumar, W. J. Zhao, A. H. Neto, J. Martin, S. Adam, B. Özyilmaz and G. Eda, *Nano Lett.*, 2014, **14**, 1909–1913.

6 B. Radisavljevic, A. Radenovic, J. Brivio, V. Giacometti and A. Kis, *Nat. Nanotechnol.*, 2011, **6**, 147–150.

7 H. Wang, H. B. Feng and J. H. Li, *Small*, 2014, **11**, 2165–2181.

8 J. Xiao, D. Choi, L. Cosimbescu, P. Koech, J. Liu and J. P. Lemmon, *Chem. Mater.*, 2010, **22**, 4522–4524.

9 U. K. Sen and S. Mitra, *ACS Appl. Mater. Interfaces*, 2013, **5**, 1240–1247.

10 H. Hwang, H. Kim and J. Cho, *Nano Lett.*, 2011, **11**, 4826–4830.

11 X. Wang, Z. Zhang, Y. Chen, Y. Qu, Y. Lai and J. Li, *J. Alloys Compd.*, 2014, **600**, 84–90.

12 H. Yu, C. Zhu, K. Zhang, Y. Chen, C. Li, P. Gao, P. Yang and Q. Ouyang, *J. Mater. Chem. A*, 2014, **2**, 4551–4557.

13 X. Y. Yu, H. Hu, Y. Wang, H. Chen and X. W. Lou, *Angew. Chem., Int. Ed.*, 2015, **54**, 7395–7398.

14 L. Yang, S. Wang, J. Mao, J. Deng, Q. Gao, Y. Tang and O. G. Schmidt, *Adv. Mater.*, 2013, **25**, 1180–1184.

15 S. Zhang, X. Yu, H. Yu, Y. Chen, P. Gao, C. Li and C. Zhu, *ACS Appl. Mater. Interfaces*, 2014, **6**, 21880–21885.

16 H. Yu, C. Ma, B. Ge, Y. Chen, Z. Xu, C. Zhu, C. Li, Q. Ouyang, P. Gao and J. Li, *Chemistry*, 2013, **19**, 5818–5823.

17 W. Jin, J. Liu, D. Chao, J. Yan, J. Lin and S. Z. Xiang, *Adv. Mater.*, 2014, **26**, 7162–7169.

18 J. Wang, C. Luo, T. Gao, A. Langrock, A. C. Mignerey and C. Wang, *Small*, 2014, **11**, 473–481.

19 L. Zhang and X. W. Lou, *Chemistry*, 2014, **20**, 5219–5223.

20 Z. Zhang, S. Pang, H. Xu, Z. Yang, X. Zhang, Z. Liu, X. Wang, X. Zhou, S. Dong and X. Chen, *RSC Adv.*, 2013, **3**, 16528–16533.

21 X. Zhu, Z. Zhen, Y. Wang, Z. Lei, A. Li and F. Huang, *Sol. Energy Mater. Sol. Cells*, 2012, **101**, 57–61.

22 J. Qian, K. J. Jiang, J. H. Huang, Q. S. Liu, L. M. Yang and Y. Song, *Angew. Chem., Int. Ed.*, 2012, **51**, 10351–10354.

23 M. Z. Xue, J. Yao, S. C. Cheng and Z. W. Fu, *J. Electrochem. Soc.*, 2006, **153**, A270–A274.

24 Z. Zhang, X. Yang, X. Wang, Q. Li and Z. Zhang, *Solid State Ionics*, 2014, **260**, 101–106.

25 Q. H. Wang, K. Kalantar-Zadeh, A. Kis, J. N. Coleman and M. S. Strano, *Nat. Nanotechnol.*, 2012, **7**, 699–712.

26 C. P. Yang, Y. X. Yin and Y. G. Guo, *J. Phys. Chem. Lett.*, 2015, **6**, 256–266.

27 *CRC Handbook of Chemistry and Physics*, ed. D. R. Lide, CRC Press, Boca Raton, FL, 82nd edn, 2001.

28 *Lange's Handbook of Chemistry*, ed. J. G. Speight, 16th edn, McGraw-Hill, New York, 2005.

29 "*Sulfur Statistics*" and "*Selenium Statistics*". *Historical Statistics for Mineral and Material Commodities in the United States*, U.S. Geological Survey, Reston, VA, 2014.

30 Material Safety Data Sheet. Acros Organics, ACR20122 (sulfur) and ACR41927 (selenium).

31 "*Sulfur*" and "*Selenium*". *Mineral Commodity Summaries 2014*, U.S. Geological Survey, Reston, VA, 2014.

32 K. V. Kranthi, S. Dhar, T. H. Choudhury, S. A. Shivashankar and S. Raghavan, *Nanoscale*, 2015, **7**, 7802–7810.

33 Q. Ji, Y. Zhang, Y. Zhang and Z. Liu, *Chem. Soc. Rev.*, 2015, **44**, 2587–2602.

34 Y. Shi, H. Li and L. J. Li, *Chem. Soc. Rev.*, 2015, **44**, 2744–2756.

35 H. F. Liu, S. L. Wong and D. Z. Chi, *Chem. Vap. Deposition*, 2015, **21**, 241–259.

36 K. J. Huang, J. Z. Zhang and Y. Fan, *Mater. Lett.*, 2015, **152**, 244–247.

37 Y. Wang, B. Qian, H. Li, L. Liu, L. Chen and H. Jiang, *Mater. Lett.*, 2015, **141**, 35–38.

38 K. Share, J. Lewis, L. Oakes, R. E. Carter, A. P. Cohn and C. L. Pint, *RSC Adv.*, 2015, **5**, 101262–101267.

39 Z. Y. Lei, S. J. Xu and P. Y. Wu, *Phys. Chem. Chem. Phys.*, 2015, **18**, 70–74.

40 L. Hao, X. Li and L. Zhi, *Adv. Mater.*, 2013, **25**, 3899–3904.

41 A. L. M. Reddy, S. R. Gowda, M. M. Shaijumon and P. M. Ajayan, *Adv. Mater.*, 2012, **24**, 5045–5064.

42 S. Selvam, B. Balamuralitharan, S. N. Karthick, A. D. Savariraj, K. V. Hemalatha, S. K. Kim and H. J. Kim, *J. Mater. Chem. A*, 2015, **3**, 10225–10232.

43 P. Humpolicek, V. Kasparkova, P. Saha and J. Stejskal, *Synth. Met.*, 2012, **162**, 722–727.

44 G. Wang, L. Zhang and J. Zhang, *Chem. Soc. Rev.*, 2012, **41**, 797–828.

45 Z. S. Wu, G. Zhou, L. C. Yin, W. Ren, F. Li and H. M. Cheng, *Nano Energy*, 2012, **1**, 107–131.

46 M. Beidaghi and Y. Gogotsi, *Energy Environ. Sci.*, 2014, **7**, 867–884.

47 L. L. Zhang, Z. Xiong and X. S. Zhao, *ACS Nano*, 2010, **4**, 7030–7036.

48 X. Kong, D. N. Lu, Z. Liu and J. Z. Wu, *Nano Res.*, 2015, **8**, 931–940.

49 Y. Shao, M. F. El-Kady, L. J. Wang, Q. Zhang, Y. Li, H. Wang, M. F. Mousavi and R. B. Kaner, *ChemInform*, 2015, **44**, 3639–3665.

50 J. Sun, Z. Li, J. Wang, Z. Wang, L. Niu, P. Gong, X. Liu, H. Wang and S. Yang, *J. Alloys Compd.*, 2013, **581**, 217–222.

51 X. Zhang, H. Zhang, C. Li, K. Wang, X. Sun and Y. Ma, *RSC Adv.*, 2014, **4**, 45862–45884.

52 O. Barbieri, M. Hahn, A. Herzog and R. Kötz, *Carbon*, 2005, **43**, 1303–1310.

53 Y. W. Zhu, S. Murali, M. Stoller, K. Ganesh, W. W. Cai, P. Ferreira, A. Pirkle, R. Wallace, K. Cychosz, M. Thommes, D. Su, E. Stach and R. Ruoff, *Science*, 2011, **332**, 1537–1541.

54 X. Lang, A. Hirata, T. Fujita and M. Chen, *Nat. Nanotechnol.*, 2011, **6**, 232–236.

55 S. C. Hong, S. Kim, W. J. Jang, T. H. Han, J. P. Hong, J. S. Oh, T. Hwang, Y. Lee, J. H. Lee and J. D. Nam, *RSC Adv.*, 2014, **4**, 48276–48284.

56 L. Wang, G. Duan, J. Zhu, S. M. Chen, X. H. Liu and S. Palanisamy, *J. Colloid Sci.*, 2016, **483**, 73–83.

57 S. Faraji and F. N. Ani, *J. Power Sources*, 2014, **263**, 338–360.

58 F. Shi, L. Li, X. L. Wang, C. D. Gu and J. P. Tu, *RSC Adv.*, 2014, **4**, 41910–41921.

59 Q. Yang, Z. Lu, J. Liu, X. Lei, Z. Chang, L. Luo and X. Sun, *Prog. Nat. Sci.*, 2013, **23**, 351–366.

60 G. A. Snook, P. Kao and A. S. Best, *J. Power Sources*, 2011, **196**, 1–12.

61 X. Chia, A. Y. Eng, A. Ambrosi, S. M. Tan and M. Pumera, *Chem. Rev.*, 2015, **115**, 11941–11966.

62 J. D. Cain, E. D. Hanson, F. Shi and V. P. Dravid, *Curr. Opin. Solid State Mater. Sci.*, 2016, **51**, 141–162.

63 G. Xiong, P. He, L. Liu, T. Chen and T. S. Fisher, *J. Mater. Chem. A*, 2015, **3**, 22940–22948.

64 M. Zhi, C. Xiang, J. Li, M. Li and N. Wu, *Nanoscale*, 2012, **5**, 72–88.

65 S. Z. Butler, S. M. Hollen, L. Cao, Y. Cui, J. A. Gupta, H. R. Gutiérrez, T. F. Heinz, S. S. Hong, J. Huang and A. F. Ismach, *ACS Nano*, 2013, **7**, 2898–2926.

66 A. Ramadoss, T. Kim, G. S. Kim and J. K. Sang, *New J. Chem.*, 2014, **38**, 2379–2385.

67 H. Wang, H. Yuan, S. S. Hong, Y. Li and Y. Cui, *Chem. Soc. Rev.*, 2015, **46**, 2664–2680.

68 R. Bose, S. K. Balasingam, S. Shin, Z. Jin, D. H. Kwon, Y. Jun and Y. S. Min, *Langmuir*, 2015, **31**, 5220–5227.

69 Y. N. Ko, S. H. Choi, S. B. Park and Y. C. Kang, *Nanoscale*, 2014, **6**, 10511–10515.

70 Z. Zhang, Y. Fu, X. Yang, Y. Qu and Z. Zhang, *ChemNanoMat*, 2015, **1**, 409–414.

71 H. Chen, Y. Xie, H. Cui, W. Zhao, X. Zhu, Y. Wang, X. Lü and F. Huang, *Chem. Commun.*, 2014, **50**, 4475–4477.

72 H. Tang, K. Dou, C. C. Kaun, Q. Kuang and S. Yang, *J. Mater. Chem. A*, 2013, **2**, 360–364.

73 R. Long and O. V. Prezhdo, *Nano Lett.*, 2016, **16**, 1996–2003.

74 A. Arora, K. Nogajewski, M. Molas, M. Koperski and M. Potemski, *Nanoscale*, 2015, **7**, 20769–20775.

75 K. J. Huang, J. Z. Zhang and Y. Fan, *Mater. Lett.*, 2015, **152**, 244–247.

76 Y. Shi, C. Hua, B. Li, X. Fang, C. Yao, Y. Zhang, Y. S. Hu, Z. Wang, L. Chen and D. Zhao, *Adv. Funct. Mater.*, 2013, **23**, 1832–1838.

77 X. Cao, Z. Yin and H. Zhang, *Energy Environ. Sci.*, 2014, **7**, 18–22.

78 Y. He, W. Chen, C. Gao, J. Zhou, X. Li and E. Xie, *Nanoscale*, 2013, **5**, 8799–8820.

79 M. F. El-Kady, S. Veronica, D. Sergey and R. B. Kaner, *Science*, 2012, **335**, 1326–1330.

80 W. Yuan, J. Chen and G. Shi, *Mater. Today*, 2014, **17**, 77–85.

81 K. J. Huang, J. Z. Zhang and J. L. Cai, *Electrochim. Acta*, 2015, **180**, 770–777.

82 S. K. Balasingam, J. S. Lee and Y. Jun, *Dalton Trans.*, 2015, **44**, 15491–15498.

83 S. K. Balasingam, J. S. Lee and Y. Jun, *Dalton Trans.*, 2016, **45**, 9646–9653.

84 X. Liu, J. Z. Zhang, K. J. Huang and P. Hao, *Chem. Eng. J.*, 2016, **302**, 437–445.

85 Z. Wang, Q. Sha, F. Zhang, J. Pu and W. Zhang, *CrystEngComm*, 2013, **15**, 5928–5934.

86 A. Banerjee, S. Bhatnagar, K. K. Upadhyay, P. Yadav and S. Ogale, *ACS Appl. Mater. Interfaces*, 2014, **6**, 18844–18852.

87 H. Peng, G. Ma, K. Sun, Z. Zhang, J. Li, X. Zhou and Z. Lei, *J. Power Sources*, 2015, **297**, 351–358.

88 N. Yu, M. Q. Zhu and D. Chen, *J. Mater. Chem. A*, 2015, **3**, 7910–7918.

89 P. Pazhamalai, K. Krishnamoorthy and J. K. Sang, *Int. J. Hydrogen Energy*, 2016, **41**, 14830–14835.

90 C. Zhang, H. Yin, M. Han, Z. Dai, H. Pang, Y. Zheng, Y. Q. Lan, J. Bao and J. Zhu, *ACS Nano*, 2014, **8**, 3761–3770.

91 X. Wang, B. Liu, Q. Wang, W. Song, X. Hou, D. Chen, Y. B. Cheng and G. Shen, *Adv. Mater.*, 2013, **25**, 1479–1486.

92   F. Cavallo and M. G. Lagally, *Soft Matter*, 2009, **6**, 439–455.

93   M. Osada and T. Sasaki, *Adv. Mater.*, 2012, **24**, 210–228.

94   V. Nicolosi, M. Chhowalla, M. G. Kanatzidis, M. S. Strano and J. N. Coleman, *Science*, 2013, **340**, 568–568.

95   Z. Fan, X. Huang, C. Tan and H. Zhang, *Chem. Sci.*, 2014, **46**, 95–111.

96   X. Yang, Z. Zhang, Y. Fu and Q. Li, *Nanoscale*, 2015, **7**, 10198–10203.

97   Y. Tang, Y. Zhang, W. Li, B. Ma and X. Chen, *Chem. Soc. Rev.*, 2015, **44**, 5926–5940.

98   P. Roy and S. Srivastava, *J. Mater. Chem. A*, 2015, **3**, 2454–2484.

99   N. Nitta, F. Wu, J. T. Lee and G. Yushin, *Mater. Today*, 2015, **18**, 252–264.

100 L. Zhang, L. Lu, D. Zhang, W. Hu, N. Wang, B. Xu, Y. Li and H. Zeng, *Electrochim. Acta*, 2016, **209**, 423–429.

101 M. Z. Xue and Z. W. Fu, *Electrochem. Commun.*, 2006, **8**, 1855–1862.

102 Y. Shi, C. Hua, B. Li, X. Fang, C. Yao, Y. Zhang, Y. S. Hu, Z. Wang, L. Chen and D. Zhao, *Adv. Funct. Mater.*, 2013, **23**, 1832–1838.

103 H. Wang, X. Wang, L. Wang, J. Wang, D. Jiang, G. Li, Y. Zhang, H. Zhong and Y. Jiang, *J. Phys. Chem. C*, 2015, **119**, 10197–10205.

104 S. Z. Kang, X. Li, J. Mu, L. Jia, Y. Yin, L. Li and Y. G. Guo, *Colloids Surf., A*, 2012, **406**, 1–5.

105 K. Klavetter, J. Pedrodesouza, A. Heller and C. B. Mullins, *J. Mater. Chem. A*, 2015, **3**, 5829–5834.

106 H. S. Im, Y. R. Lim, J. C. Yong, J. Park, E. H. Cha and S. K. Hong, *J. Phys. Chem. C*, 2014, **118**, 21884–21888.

107 F. Chen, J. Wang, B. Li, C. Yao, H. Bao and Y. Shi, *Mater. Lett.*, 2014, **136**, 191–194.

108 J. Yao, B. Liu, S. Ozden, J. Wu, S. Yang, M. T. F. Rodrigues, K. Kalaga, P. Dong, P. Xiao and Y. Zhang, *Electrochim. Acta*, 2015, **176**, 103–111.

109 L. Ma, X. Zhou, L. Xu, X. Xu, L. Zhang and W. Chen, *J. Power Sources*, 2015, **285**, 274–280.

110 Y. Lai, W. Chen, Z. Zhang, Y. Gan, X. Yang and J. Li, *RSC Adv.*, 2016, **6**, 19843–19847.

111 B. Mendoza-Sánchez, J. Coelho, A. Pokle and V. Nicolosi, *Electrochim. Acta*, 2016, **192**, 1–7.

112 Y. Liu, M. Zhu and D. Chen, *J. Mater. Chem. A*, 2015, **3**, 11857–11862.

113 J. Choi, J. Jin, I. G. Jung, J. M. Kim, H. J. Kim and S. U. Son, *Chem. Commun.*, 2011, **47**, 5241–5243.

114 L. Zhang, L. Lu, D. Zhang, W. Hu, N. Wang, B. Xu, Y. Li and H. Zeng, *Electrochim. Acta*, 2016, **209**, 423–429.

115 Z. Zhang, X. Zhao and J. Li, *Electrochim. Acta*, 2015, **176**, 1296–1301.

116 Y. Wang, B. Qian, H. Li, L. Liu, L. Chen and H. Jiang, *Mater. Lett.*, 2015, **141**, 35–38.

117 H. T. Kwon and C. M. Park, *J. Power Sources*, 2014, **251**, 319–324.

118 J. M. Tarascon and M. Armand, *Nature*, 2001, **414**, 359–367.

119 W. Qin, T. Chen, B. Hu, Z. Sun and L. Pan, *Electrochim. Acta*, 2015, **173**, 193–199.

120 P. Ge and M. Fouletier, *Solid State Ionics*, 1988, **s 28–30**, 1172–1175.

121 M. M. Doeff, Y. Ma, S. J. Visco and L. C. Dejonghe, *J. Electrochem. Soc.*, 1993, **140**, 169–170.

122 K. Share, J. Lewis, L. Oakes, R. E. Carter, A. P. Cohn and C. L. Pint, *RSC Adv.*, 2015, **5**, 101262–101267.

123 Y. Kim, K. Ha, M. Oh and K. Lee, *Chem. – Eur. J.*, 2014, **20**, 11980–11992.

124 Y. N. Ko, S. H. Choi, S. B. Park and Y. C. Kang, *Nanoscale*, 2014, **6**, 10511–10515.

125 H. Wang, X. Lan, D. Jiang, Y. Zhang, H. Zhong, Z. Zhang and Y. Jiang, *J. Power Sources*, 2015, **283**, 187–194.

126 Y. Kim, Y. Kim, Y. Park, N. J. Yong, Y. J. Kim, N. S. Choi and K. T. Lee, *Chem. Commun.*, 2014, **46**, 50–53.

127 K. Share, J. Lewis, L. Oakes, R. E. Carter, A. P. Cohn and C. L. Pint, *RSC Adv.*, 2015, **5**, 101262–101267.

128 Z. Zhang, X. Yang, Y. Fu and K. Du, *J. Power Sources*, 2015, **296**, 2–9.

129 S. H. Choi and Y. C. Kang, *Nanoscale*, 2016, **8**, 4209–4216.

130 X. Yang, Z. Zhang, Y. Fu and Q. Li, *Nanoscale*, 2015, **7**, 10198–10203.

131 Y. Zhang, Z. Liu, H. Zhao and Y. Du, *RSC Adv.*, 2016, **6**, 1440–1444.

132 Z. Zhang, X. Zhao and J. Li, *Electrochim. Acta*, 2015, **176**, 1296–1301.

133 Z. Zhang, X. Yang and Y. Fu, *RSC Adv.*, 2016, **6**, 12726–12729.

134 C. Wan, Y. N. Regmi and B. M. Leonard, *Angew. Chem., Int. Ed.*, 2014, **53**, 6407–6410.

135 C. Wei, A. M. Asiri, X. Sun, L. Qian, Z. Xing and K. A. Alamry, *Appl. Catal., B*, 2015, **164**, 144–150.

136 X. Peng, Y. Yan, X. Ge, Z. Liu, J. Y. Wang, W. Xin, X. Peng, Y. Yan, X. Ge and Z. Liu, *Appl. Catal., B*, 2014, **s 154–155**, 232–237.

137 T. W. Lin, C. J. Liu and J. Y. Lin, *Appl. Catal., B*, 2013, **134–135**, 75–82.

138 S. Wirth, F. Harnisch, M. Weinmann and U. Schröder, *Appl. Catal., B*, 2012, **126**, 225–230.

139 A. Moya, A. Cherevan, S. Marchesan, P. Gebhardt, M. Prato, D. Eder and J. J. Vilatela, *Appl. Catal., B*, 2015, **179**, 574–582.

140 T. W. Lin, C. J. Liu and C. S. Dai, *Appl. Catal., B*, 2014, **s 154–155**, 213–220.

141 Y. Huang, H. Lu, H. Gu, J. Fu, S. Mo, C. Wei, Y. E. Miao and T. Liu, *Nanoscale*, 2015, **7**, 18595–18602.

142 Y. Shi, C. Hua, B. Li, X. Fang, C. Yao, Y. Zhang, Y. S. Hu, Z. Wang, L. Chen and D. Zhao, *Adv. Funct. Mater.*, 2013, **23**, 1832–1838.

143 U. Maitra, U. Gupta, M. De, R. Datta, A. Govindaraj and D. C. N. R. Rao, *Angew. Chem., Int. Ed.*, 2013, **52**, 13057–13061.

144 H. Wang, Z. Lu, D. Kong, J. Sun, T. M. Hymel and Y. Cui, *ACS Nano*, 2014, **8**, 4940–4947.

145 X. Fan, L. Zhang, W. Min, W. Huang, Y. Zhou, M. Li, R. Cheng and J. Shi, *Appl. Catal., B*, 2016, **182**, 68–73.

146 Q. Liu, J. Tian, W. Cui, P. Jiang, N. Cheng, A. M. Asiri and X. Sun, *Angew. Chem.*, 2014, **126**, 6828–6832.

147 P. Jiang, Q. Liu, Y. H. Liang, A. Asiri and X. P. Sun, *Angew. Chem., Int. Ed.*, 2014, **53**, 12855–12859.

148 Y. Huang, Y. Miao, J. Fu, S. Mo, C. Wei and T. Liu, *J. Mater. Chem. A*, 2015, **3**, 16263–16271.

149 Y. Huang, Y. Miao, J. Fu, S. Mo, C. Wei and T. Liu, *J. Mater. Chem. A*, 2015, **3**, 16263–16271.

150 X. Hu, Z. Wei, X. Liu, Y. Mei and Y. Huang, *Chem. Soc. Rev.*, 2015, **44**, 2376–2404.

151 J. Shaw, H. L. Zhou, Y. Chen, N. Weiss, Y. Liu, Y. Huang and X. F. Duan, *Nano Res.*, 2014, **7**, 511–517.

152 L. Jia, X. Sun, Y. Jiang, S. Yu and C. Wang, *Adv. Funct. Mater.*, 2014, **25**, 1814–1820.

153 S. Xu, Z. Lei and P. Wu, *J. Mater. Chem. A*, 2015, **3**, 16337–16347.

154 Y. Zhang, L. Zuo, L. Zhang, Y. Huang, H. Lu, W. Fan and T. Liu, *ACS Appl. Mater. Interfaces*, 2016, **11**, 7077–7085.

155 D. Kong, H. Wang, Z. Lu and Y. Cui, *J. Am. Chem. Soc.*, 2014, **136**, 4897–4900.

156 W. Zhao, B. Dong, Z. Guo, G. Su, R. Gao, W. Wang and L. Cao, *Chem. Commun.*, 2016, **52**, 9228–9231.

157 L. Xiao, Z. Li, X. Zang, X. Li and H. Zhu, *ACS Appl. Mater. Interfaces*, 2016, **8**, 10866–10873.

158 C. Tsai, K. Chan, F. Abildpedersen and J. K. Nørskov, *Phys. Chem. Chem. Phys.*, 2014, **16**, 13156–13164.

159 X. Zhou, J. Jiang, T. Ding, J. Zhang, B. Pan, J. Zuo and Q. Yang, *Nanoscale*, 2014, **6**, 11046–11051.

160 C. Xu, S. Peng, C. Tan, H. Ang, H. Tan, H. Zhang and Q. Yan, *J. Mater. Chem. A*, 2014, **2**, 5597–5601.

161 A. Ambrosi, Z. Sofer and M. Pumera, *Chem. Commun.*, 2015, **51**, 8450–8453.

162 Z. Gholamvand, D. Mcateer, C. Backes, N. Mcevoy, A. Harvey, N. C. Berner, D. Hanlon, C. Bradley, I. Godwin and A. Rovetta, *Nanoscale*, 2016, **8**, 5737–5749.

163 C. H. Mu, H. X. Qi, Y. Q. Song, Z. P. Liu, L. X. Ji, J. G. Deng, Y. B. Liao and F. Scarpa, *RSC Adv.*, 2015, **6**, 23–30.

164 X. Liu, J. Z. Zhang, K. J. Huang and P. Hao, *Chem. Eng. J.*, 2016, **302**, 437–445.

165 Z. Liu, N. Li, H. Zhao and Y. Du, *J. Mater. Chem. A*, 2015, **3**, 19706–19710.

166 R. I. Romanov, V. Y. Fominski, A. V. Shelyakov and G. V. Golubkov, *Russ. J. Phys. Chem. B*, 2016, **10**, 238–244.

167 Y. Liu, L. Ren, Z. Zhang, X. Qi, H. Li and J. Zhong, *Sci. Rep.*, 2016, **6**, 1–9.

168 B. Qu, X. Yu, Y. Chen, C. Zhu, C. Li, Z. Yin and X. Zhang, *ACS Appl. Mater. Interfaces*, 2015, **7**, 14170–14175.

169 S. H. Lin and J. L. Kuo, *Phys. Chem. Chem. Phys.*, 2015, **17**, 29305–29310.

170 V. Kiran, D. Mukherjee, R. N. Jenjeti and S. Sampath, *Nanoscale*, 2014, **6**, 12856–12863.

171 U. Gupta, B. S. Naidu, U. Maitra, A. Singh, S. N. Shirodkar, U. V. Waghmare and C. N. R. Rao, *APL Mater.*, 2014, **2**, 1167–1178.

172 Y. Huang, Y. Miao, J. Fu, S. Mo, C. Wei and T. Liu, *J. Mater. Chem. A*, 2015, **3**, 16263–16271.

173 Y. Huang, H. Lu, H. Gu, J. Fu, S. Mo, C. Wei, Y. E. Miao and T. Liu, *Nanoscale*, 2015, **7**, 18595–18602.

174 S. N. Grigoriev, V. Y. Fominski, R. I. Romanov, M. A. Volosova and A. V. Shelyakov, *Thin Solid Films*, 2015, **592**, 175–181.

175 X. Zhou, Y. Liu, H. Ju, B. Pan, J. Zhu, T. Ding, C. Wang and Q. Yang, *Chem. Mater.*, 2016, **28**, 1838–1846.

176 B. Qu, Q. Ouyang, X. Yu, W. Luo, L. Qi and Y. Chen, *Phys. Chem. Chem. Phys.*, 2015, **17**, 6036–6043.

177 S. Mao, Z. Wen, S. Ci, X. Guo, K. Ostrikov and J. Chen, *Small*, 2014, **11**, 414–419.

178 D. Xie, W. Tang, Y. Wang, X. Xia, Y. Zhong, D. Zhou, D. Wang, X. Wang and J. Tu, *Nano Research*, 2016, **9**, 1618–1629.

179 W. Gao, Y. Miao, Z. Chao, Y. Zhe, Z. Liu, W. T. Weng and T. Liu, *ACS Appl. Mater. Interfaces*, 2013, **5**, 7584–7591.

180 S. Rafiei, B. Noroozi, S. Arbab and A. K. Haghi, *Chin. J. Polym. Sci.*, 2014, **32**, 449–457.

181 D. Kong, H. Wang, J. J. Cha, M. Pasta, K. J. Koski, J. Yao and Y. Cui, *Nano Lett.*, 2013, **13**, 1341–1347.

182 L. Jia, X. Sun, Y. Jiang, S. Yu and C. Wang, *Adv. Funct. Mater.*, 2014, **25**, 1814–1820.

This journal is © The Royal Society of Chemistry 2017